Figueira, D.; Sena-Cruz, J.; Pereira, E.; Valente, I.; Barros, J.; Castro, F.; Soares, D. (2019) "Influence of service temperature on shear creep behaviour of a rigid low-density closed-cell PIR foam" Construction & Building Materials, 225: 1052–1063.
DOI: 10.1016/j.conbuildmat.2019.07.337

INFLUENCE OF SERVICE TEMPERATURE ON SHEAR CREEP BEHAVIOUR OF A RIGID LOW-DENSITY CLOSED-CELL PIR FOAM

Diogo Figueira[1], José Sena-Cruz[2]*, Eduardo Pereira[3], Isabel Valente[4], Joaquim Barros[5], Fernando Castro[6], Delfim Soares[7]

Abstract: An experimental campaign was carried out to assess shear creep behaviour of a rigid low-density closed-cell polyisocyanurate (PIR) foam. Two service temperature values were considered, 20 ºC and 30 ºC, and the applied stresses ranged between 20% and 60% of the corresponding shear strength. The results showed that a stress amplitude of 30% was enough to cause nonlinear creep response. Furthermore, creep deformations were slightly smaller in the tests at 30 ºC, a fact that matched the viscoelastic response of the PIR foam obtained from DMA testing. Finally, creep prediction curves were calibrated through an analytical approach based on the Findley's power law.

Keywords: Polymeric foams; Polyisocyanurate (PIR); Shear creep; Temperature; Findley's power law.

[1] Researcher, ISISE, IB-S, University of Minho, School of Engineering, Campus de Azurém, 4800-058 Guimarães, Portugal. Email: dfigueira@civil.uminho.pt

[2] Associate Professor, ISISE, IB-S, University of Minho, School of Engineering, Campus de Azurém, 4800-058 Guimarães, Portugal. Email: jsena@civil.uminho.pt *Corresponding Author

[3] Assistant Professor, ISISE, IB-S, University of Minho, School of Engineering, Campus de Azurém, 4800-058 Guimarães, Portugal. Email: eduardo.pereira@civil.uminho.pt

[4] Assistant Professor, ISISE, IB-S, University of Minho, School of Engineering, Campus de Azurém, 4800-058 Guimarães, Portugal. Email: isabelv@civil.uminho.pt

[5] Full Professor, ISISE, IB-S, University of Minho, School of Engineering, Campus de Azurém, 4800-058 Guimarães, Portugal. Email: barros@civil.uminho.pt

[6] Full Professor, CT2M, Department of Mechanical Engineering, University of Minho, 4800-058 Guimarães, Portugal. E-mail: fcastro@dem.uminho.pt

[7] Assistant Professor, CMEMS, Department of Mechanical Engineering, University of Minho, 4800-058 Guimarães, Portugal. E-mail: dsoares@dem.uminho.pt

Figueira, D.; Sena-Cruz, J.; Pereira, E.; Valente, I.; Barros, J.; Castro, F.; Soares, D. (2019) "Influence of service temperature on shear creep behaviour of a rigid low-density closed-cell PIR foam" Construction & Building Materials, 225: 1052–1063.
DOI: 10.1016/j.conbuildmat.2019.07.337

1. INTRODUCTION

The Polyisocyanurate (PIR) foam polymer differs from the traditional Polyurethane (PUR) foam in the stronger molecular structure that is achieved in its manufacturing procedure, consisting on highly cross-linked isocyanurate rings [1,2]. These enhancements are traduced in the thermal stability, flame retardance and mechanical behaviour of PIR [3,4], turning it more suitable than PUR to be used as a foam material in situations in which these properties play a relevant role [5,6].

Polymeric foams are commonly used as core materials of composite sandwich panels in civil and military structural applications [7,8]. In the former applications, which are the scope of the present research, the foam material should combine stiffness with low thermal conductivity, fire resistance performance and lightness [9,10]. Having these properties, the foam maintains the integrity during its service life, acts as a thermal insulation material and fire retardant, and has minor impact on the total weight of the structure [11,12]. These requirements explain the use of rigid closed-cell polymeric foams (as PUR and PIR) in the sandwich panels, which are stiffer and more heat flow resistant when compared to flexible open-cell foams [13].

When the sandwich panels are used as structural elements in a floor or a wall, the foam is mainly subjected to shear stresses, whose influence in its integrity should be considered when the panels are being designed [14]. In this context, the foam density usually depends on the configuration of the panel and the number of ribs providing shear strength. In the panel structural design, the adoption of with ribs and low-density foams is often preferred, as opposed to the solution where only high-density foams are adopted and ribs are absent. This is the case in the work reported in [7], where a sandwich panel consisting of thin, interconnecting, fibre reinforced polymer (FRP) facing sheets that form a bidirectional gridwork infilled with a polymeric foam, is described as the optimal solution. Moreover, due to significant permanent loads on the panels, the shear creep behaviour of the foam and its deformations should be accounted for and checked as well [15]. In this matter, the influence of temperature in the shear creep effect can be significant [16].

Typically, the main function expected for PIR foams is thermal insulation. Therefore, publications concerning their thermal response and fire resistance are abundant in literature [17–24]. However, other properties of PIR still need to be assessed, particularly regarding its structural integrity and mechanical behaviour as a foam material in composite structural sandwich panels. This paper intends to provide new knowledge within this scope. At first, a literature review is made in order to provide the background on the relevant treated subjects. Then, the experimental program developed is detailed, and its results are presented and discussed. The results obtained are

later used to calibrate modelling parameters of an analytical approach for predicting shear creep deformation of PIR when subjected to expected stress levels and temperatures. Finally, the main conclusions of the work are summarized.

2. LITERATURE REVIEW

Several studies were carried out to assess the compressive (e.g. [25,26]), tensile (e.g. [27]) and shear strengths (e.g. [28]) of PUR foam. Creep behaviour of PUR is highlighted in the work of Huang and Gibson [29], which considered the empirical Findley's power law [30,31] for the modelling of the PUR creep behaviour. More recently, El Ghezal *et al.* [32] modelled PUR creep through a micromechanical approach. The temperature effect on the mechanical properties of PUR is already well described in the works of Crawford *et al.* [33] and Garrido *et al.* [34]. The influence of temperature on the creep behaviour of PUR subjected to compression and shear was investigated by Briody *et al.* [35] and Garrido *et al.* [16], respectively. A significant influence was observed in both studies.

Some research works were designed to assess the mechanical properties of PIR for compression and tensile behaviour. Javni *et al.* [36] assessed the thermal response of PIR along with its compressive strength. Later, Stirna *et al.* [37] developed an experimental campaign to observe PIR behaviour subjected to compressive and tensile stresses, with deformations measured in the directions parallel and perpendicular to the applied load. In the last years, some further developments were carried out, particularly the study of Andersons *et al.* [38] in which PIR stiffness and strength were analysed considering their anisotropic performance. Continuing their research, the same authors [39] evaluated the fracture toughness through experimental tensile tests, and the obtained results were considered in a micromechanical approach that accounted for the microscopic properties of the PIR foam.

In terms of PIR shear behaviour and shear creep behaviour, information available in literature is absent. This paper presents an experimental campaign aiming to obtain results on PIR shear strength, shear creep behaviour and the influence of temperature in its creep response.

3. EXPERIMENTAL PROGRAM

The experimental program carried out in this study is encompassed in the research project "Easyfloor–Development of composite sandwich panels for building floor rehabilitation". The sandwich panels developed in

the project contain several improvements over the most common solutions used nowadays [40]. In this context, PIR was included in the sandwich panels as the foam core material due to its enhanced insulation properties.

One of the main tasks in this research project is the individual mechanical characterization of the materials forming the sandwich panel. Thus, the present experimental program on the PIR foam comprised two main types of tests: i) failure tests to assess the behaviour of PIR under pure quasi-static monotonic-instantaneous shear loading; and, ii) creep tests, where PIR is subjected to a pure shear constant load over time. The load applied in the creep tests is a percentage of the average ultimate load obtained in instantaneous failure tests. The objective of the creep tests is to determine PIR creep response for different load amplitudes and service temperatures.

Prior to the shear tests on the PIR foam (failure and creep), which were designed to fulfil the principal objectives of this study, some other tests were carried out to characterize the PIR material. All the PIR specimens tested correspond to a rigid low-density closed-cell foam. The foam manufacturing was implemented through the mechanical mixing (at 3000 rpm and 20 ºC) of isocyanate, polyol, surfactant, catalysts, water and the blowing agent (CO2). The isocyanate index is 160. According to the technical datasheet of the product, the typical properties of this PIR foam are: density of 40 - 50 kg/m^3 (EN 1602); thermal conductivity <0.024 W·K-1/m (EN 12667); closed-cell content >90% (ISO 4590); compressive strength >270 kPa (EN 826); dimensional stability (70 °C, 90% RH / -20 °C) ≤0.5% / ≤1% (EN 1604); fire behaviour E(Euroclass, EN13501-1), B2 (Building Material, DIN 4102-1); water absorption ≤0.5 kg/m^2 (EN 1609).

3.1 Material characterization

For the material characterization of the PIR foam, compression and direct tensile tests were carried out following the applicable normative rules. For the compression tests, the specifications of standard ASTM C365 [41] were adopted, resulting in an average compressive strength of 0.22 MPa (CoV = 10.67 %) and elastic modulus of 5.81 MPa (CoV = 11.53 %) for the 5 specimens tested (see **Figure 1**(a)). The direct tensile tests followed the guidelines on the standard ASTM C297 [42], and an average direct tensile strength of 0.22 MPa (CoV = 15.52 %) and elastic modulus of 4.79 MPa (CoV = 10.03 %) were obtained for the 5 specimens tested (**Figure 1**(b)). The uniaxial compression and tensile tests were performed parallel to the foam rise direction.

The viscoelastic thermal response of the material was measured through a classic Dynamic Mechanical Analysis (DMA) test [34], in order to evaluate the effect of temperature on PIR creep. In this test, prismatic specimens with 10 mm width, 4 mm thickness and 60 mm length were used. The dynamic load was applied in a

dual cantilever setup at a frequency of 1 Hz, and the samples were heated at a rate of 1 ºC/min, under an inert atmosphere (N2), from -50 ºC to 200 ºC.

Figure 2 shows the typical results obtained in the DMA tests performed on PIR foam specimens, in terms of the evolution of the storage modulus *E*', the loss modulus *E*" and the loss factor tan (δ), where δ = arctan (*E*" / *E*'). With the temperature increasing between -50 ºC and 200 ºC, a couple aspects can be identified that sustain the PIR foam as a polymer with an increased thermal stability, as follows:

- Firstly, a sudden drop in the storage modulus is not seen;
- Secondly, a maximum peak value is not observed for the loss modulus, which seems to decrease continuously with temperature. Furthermore, that continuous decrease with temperature is more pronounced for temperatures approximately between 0 ºC and 40 ºC, matching a wide range of in-service temperature values that are expected in a sandwich panel;
- Thirdly, regarding the loss factor, it shows a slight continuous and approximately linear decrease for temperatures varying between 0 ºC and 40 ºC, reflecting the behaviour observed for *E'* and *E"*.

These statements match the observations of Javni *et al.* [36] concerning DMA tests carried out in rigid foams with a high isocyanate index. A high level of isocyanate is a characteristic of the PIR foams, and it is responsible for their strong molecular structure consisting on highly cross-linked isocyanurate rings. The results of **Figure 2** also resemble those achieved in DMA tests on thermoset polymers with crystalline structure [43], in which the molecules are arranged in an almost perfectly regular and periodic form.

Differences can be noticed when comparing the results of the present DMA tests (in PIR specimens) with PUR results available in literature [34], for the same temperature range (-50 ºC to 200 ºC): i) the rigid PUR foam has a typical sudden decrease in *E*'; and ii) *E*" continuously increases in the range of common in-service temperatures until a maximum peak is reached. A significant continuous reduction trend in storage modulus from the beginning to the end of the temperature range tested is observed, which means that PIR becomes more deformable with increasing temperature, in terms of elastic response. However, the loss modulus shows a decreasing trend with increasing temperature, indicating a reduction in viscoelasticity as temperature increases - the loss factor values have varied positively for PUR (+60%) and negatively for PIR (-33%). This fact may indicate an overall higher thermal stability of PIR within frequent in-service temperatures.

3.2 Monotonic-instantaneous shear tests up to the failure

The shear tests up to the failure on PIR followed the recommendations of ASTM C273 [44] and ISO 1922 [45]. The test fixture developed and the test configuration are illustrated in **Figure 3**(a) and **Figure 3**(b), respectively. As can be seen, two of the PIR faces are bonded to "L" shape elements made of two UNP 120 steel profiles. 3-dimensional bearing joints were used to avoid bending moments in the system. These joints ensure the verticality of the load line of action and the absence of bending moment transmission at both supports. Then, with the plates moving in opposite directions, away from each other, a transverse displacement (distortion) of the planes parallel to the bonded faces of the PIR foam is imposed (see **Figure 3**(b)).

The PIR foam was bonded to the UNP120 steel profiles with "Sika 32 EF", which is a two-component polyurethane adhesive. Initially, the steel profiles were cleaned with acetone. Then, the two components of the adhesive were mixed and applied to both the steel profiles and the PIR specimens faces. At first, while on steel profile was resting horizontally, one face of PIR was glued to it. Soon after, the other steel profile was placed on the free top face of PIR. Consequently, a slight compression was applied on the foam due to the steel profile self-weight. Simultaneously, the adhesive in excess emanating from the bonding was removed. Finally, the specimens were stored into a climatic chamber, with controlled temperature (20 ºC) and relative humidity (55%). Although only 4 hours were specified as enough curing period by the adhesive's manufacturer technical data, the specimens rested in the climatic chamber for 1 to 7 days until they were tested.

Prismatic specimens with 360 mm length, 120 mm width and 30 mm thickness were used. In total, 6 specimens (F1 to F6) were tested in quasi-static monotonic-instantaneous loading up to failure, under displacement control at a rate of 0.50 mm/min, in a universal testing machine. One LVDT was used to record the shear displacement δ developed between the plates, as shown in **Figure 3**(b). The LVDT has a measuring range of ±25 mm and a linearity error of ±0.12 mm. The applied force was measured using a load cell of 200 kN (±0.12 kN).

The geometry and dimensions defined for the specimens meet the specifications of the standards ASTM C273 [44] and ISO 1922 [45]. The standards prescribe that the width b should be higher than 50 mm, so that a good adhesion of the PIR to the plates can take place. For the specimen length L, the condition $L \geq 12 \times t$ is meet, where t is the specimen thickness. This latter condition minimizes the effect of the secondary (tensile) stresses at the specimen ends. Consequently, the applied transverse displacement can inflict pure shear along most of the foam length and shear failure is most likely to occur, represented by a diagonal crack crossing the specimen's

core. In this context, the standards state that tests which portray a cohesive failure of the adhesive, or of the PIR foam in the contact area with the adhesive, should be rejected.

The appropriateness of the setup of **Figure 3**, along with the foam specimen dimensions specified by the standards, was tested by the authors in a previous work [46], where shear failure occurred in 4 of the total 6 specimens assessed. In that experimental campaign, the principal strain patterns were measured through Digital Image Correlation (DIC), and pure shear could be depicted at most of the specimen's length. At the end, these tests allow the determination of the PIR foam mechanical properties, according to Equations (1) to (3),

$$\tau_{u} = \frac{F_{u}}{L \times b} \tag{1}$$

$$\gamma = \frac{\delta_{u}}{t} \tag{2}$$

$$G = \frac{\Delta\tau}{\Delta\gamma} \tag{3}$$

where τ_u is the ultimate shear strength, γ_u is the ultimate shear strain, G is the shear modulus, F_u is the maximum force value measured and δ_u its corresponding shear displacement. According to ASTM C273 [44], the shear modulus G should be calculated as the "slope of the initial portion" of the shear stress-strain curve. In the present study, G is calculated in the interval between $\gamma = 0.01$ and $\gamma = 0.025$.

3.3 Shear creep tests

For the shear creep tests, a new test setup was specifically developed in the present study, since a constant shear stress over time is to be applied on the PIR foam. **Figure 4** depicts the outlook of the test setup and its main features:

- Additionally to the LVDT, shear displacement was also measured through a dial gauge attached to the steel UNP120 profiles supporting the PIR foams (see **Figure 4**(a)). The LVDT is placed in one face of the test fixture and the dial gauge on the opposite face. The dial gauge was added, as a redundant measuring system, because the long duration of the creep tests increased the probability of a failure occurring in the data acquisition system associated with the LVDTs;

- The top (superior) bearing joint of the test fixture is connected to a UNP200 steel beam in equilibrium (see **Figure 4**(b)). The beam is linked (through steel chains) to the bearing joint on one end and at the other end is loaded with rock blocks (sustained load). In turn, the rock blocks were piled in order to reach the intended creep load on the PIR foam specimens. Therefore, weight of all the components of the testing system causing load was considered in the estimation of the creep load to be applied, namely the steel beam and steel plates;
- Room temperature and relative humidity RH were maintained approximately constant throughout the tests, by executing the tests into a climatic chamber containing a heating/refrigeration system.

A total of 12 specimens were tested: i) 6 at a room temperature equal to 20 ± 1.5 ºC (with RH = 55 ± 6%) and subjected to 3 load amplitudes (20%, 40% and 60% of the average shear strength measured in the shear tests up to the failure); ii) the other 6 specimens were tested at 30 ± 1.5 ºC (RH = 55 ± 6%) and subjected to 3 load amplitudes as well (20%, 30% and 40% of the average shear strength). Thus, 2 specimens were considered for each test series, so that variability could be taken into account. Temperature ranging between 20 ºC and 30 ºC is very common in temperature-controlled environments, like residential and office buildings. The load levels match the ones considered in research works [16,29] available in literature that assessed the shear creep behaviour of PUR (10% to 40% of the average shear strength). The 60% level was added in order to observe if creep failure could occur.

3.4 Post-shear creep tests

Six months after the conclusion of shear creep tests at 30 ºC, the 6 specimens were subjected to a monotonic-instantaneous shear load up to failure. The setup and procedure implemented in these tests are like the tests described in Section 3.2. This option aimed at assessing post-shear creep behaviour of these specimens and compare with the ones that did not suffer creep effects.

Finally, it should be mentioned that all the tests, namely, monotonic-instantaneous shear tests, shear creep tests shear and post-shear creep tests were performed with the foam rise direction perpendicular to the steel plates.

4. RESULTS

The results obtained in the monotonic-instantaneous shear tests up to failure and the shear creep tests are presented and analysed. Since the displacements measured in the LVDTs and in the dial gauges were very similar, only the first ones were used for the evaluation of the shear strains.

4.1 Monotonic-instantaneous shear tests up to failure

In the shear tests up to failure performed on the 6 PIR foam specimens, two failure modes were identified (**Figure 5**):

- The first failure mode – FM1 – (**Figure 5**(a)) is characterized by a shear crack parallel to the steel plates (UNP profiles – see **Figure 3**) at the interface between PIR foam and steel. In all the tests that portrayed this failure mode, the crack arose in the vicinity of the contact area of the PIR foam with the adhesive, while the adhesive itself remained intact. In general, at the bonded zone the adhesive filled the open cells and voids of the PIR and, consequently, the specimen strength is positively affected around the contact area with the adhesive. This explains the existence of a thin layer of PIR foam attached to the UNP profiles. The crack always started at the extremities, since the boundary conditions caused tensile stress concentrations near the steel plates, [46]. Then, the crack evolved along the interface PIR/steel plates;
- The second failure mode – FM2 – (**Figure 5**(b)) is another type of cohesive shear failure that PIR has experienced, characterized by the formation of a shear crack, transverse to the steel plates, at approximately specimen's half-length. The crack is diagonal (≈45º to the load line of action) due to the pure shear stress state generated by the test configuration, which inflict an inclined principal tensile stress in the foam (see in [46]).

Figure 6 shows the shear stress *versus* strain ($\tau - \gamma$) curves obtained in the 6 shear tests performed. Half of the specimens experienced failure mode FM1 and at sremaining ones FM2:

- In the case of FM2, the typical mechanical response **[28,34]** of a polymeric foam subjected to shear stress state can be recognized: i) an initial linear elastic branch, ii) a non-linear phase, and iii) a hardening elasto-plastic linear branch. The transverse shear failure takes place when the maximum shear strain of the foam is reached. This failure mode is brittle and occurred suddenly;

- Some differences can be perceived in the $\tau - \gamma$ curve of the specimens that depicted FM1. In these tests, the non-linear phase ii) does not stabilize into the hardening elasto-plastic phase iii), denoting that the shear crack parallel to the steel plates continues to grow until the specimen collapses. Here, stiffness degradation caused by cracking is governed by the shear crack parallel to the steel plates in the vicinity of the contact area between the PIR foam and the adhesive.

Table 1 presents the main results acquired in the tests. Considering only the specimens that displayed the failure mode FM2 (transverse shear crack), the average values were: i) shear strength τ_u = 0.19 MPa; ii) shear modulus G = 2.77 MPa; and iii) ultimate shear strain γ_u = 0.193. Moreover, a small variability can be verified in failure mode FM2 test results. In contrast, the tests that showed failure mode FM1 only have a small variability in the G modulus, since cracking has not yet appeared (elastic phase). In those tests, the average values of τ_u and γ_u were significantly lower.

As was explained in Section 2, no data could be found so far in literature, regarding shear strength of a PIR foam, to be compared with the results of **Table 1**. Shear tests were performed on PUR foam having a higher density: 87.4 kg/m^3 in tests performed by Garrido *et al.* [16] and 62 kg/m^3 in Witkiewicz and Zielinski [28] tests, in which the obtained shear strength average values were 0.32 MPa and 0.35 MPa, respectively.

4.2 Shear creep tests

The reference shear strength τ_u value of **Table 1** used for the shear creep tests was 0.19 MPa, the average value obtained in the tests which experienced cohesive transverse shear failure (FM2). Tests where a crack parallel to the steel plates (FM1) was formed were not considered, since this type of failure mode is not governed by the shear strength, as expected in a pure shear test.

The evolution of the PIR foam shear strain (γ) over time is illustrated in **Figure 7** for the different load amplitudes applied. Creep compliance (J), strain per unit of stress ($J = \gamma / \tau$), evolution is depicted in **Figure 8**. For a better understanding, **Table 2** (for the specimens at 20 ºC) and **Table 3** (for the specimens at 30 ºC) include the values acquired at the loading instant γ_e, just before unloading γ_c, after unloading γ_{un} and at the end of the test γ_{end}. Moreover, **Table 2** and **Table 3** also include the expected elastic shear strain, $\gamma_{e,expected}$, calculated considering the average value of G = 2.77 MPa from **Table 1**. Specimens at 20 ºC were unloaded at 2184 hours and the corresponding tests were completed at 3168 hours, while the ones settled at 30 ºC were unloaded at 3000 hours

and tests were concluded at 4080 hours. This difference between the tests at 20 ºC and at 30 ºC was implemented so that unloading at different ages (2184 hours and 3000 hours) could be tested.

During some periods, technical problems occurred and for that reason no displacement values on the specimens were measured. Those gaps can be seen in the graphs of **Figure 7** and **Figure 8** and correspond in the 20 ºC tests to the intervals: 1005 – 1497 and 2682 – 2861 hours. In the 30 ºC tests the gaps can be found in the following intervals: 786 – 818, 1479 – 1853 and 3328 – 3840 hours.

All the tests revealed the first 2 stages of the typical creep material behaviour [47]:

- Until approximately t = 200 hours, primary creep, in which the strain rate is high due to the deformation caused by the internal rearrangement of the material microstructure. This rearrangement is also the reason why the strain rate decreased with time;
- Then, the strain rate diminished to a minimum and became approximately constant as the secondary stage of creep began. The internal material microstructure does not change significantly at this stage.

In the third stage of creep, characterized by an exponential growth of deformation, the applied load inflicts damage in the material and failure is expected to occur. This third stage was not observed in the tests carried out and none of the specimens failed due to creep. This evidence reinforces the idea that PIR is an enhanced foam material, since failure was detected in the recent work of Garrido *et al.* [16] on a rigid high-density (ρ = 87.4 kg/m^3) closed-cell PUR foam. The PUR specimen that failed in that study was subjected to a creep load corresponding to 44% of the shear strength and at 28 ºC. That specimen attained creep shear strains of γ = 0.0543 (between measurements taken after 402 and 477 hours of creep), which exceeded the average failure strain reported for that foam in the static failure tests (γ = 0.043). Those load *versus* temperature conditions are not as severe as the ones implemented in the present experimental campaign, where a maximum creep shear strain of γ = 0.134 was attained at 2184 hours, less than the ultimate shear strain measured in the static tests (γ = 0.193).

The shear strain values and the strain rate always increased with the load amplitude applied. Furthermore, the results obtained were very similar for tests with the same load amplitude and room temperature, except for the tests on specimens subjected to 60% of the shear strength. After unloading, the influence of load amplitude was also relevant, as the absolute value of the strain rate was higher on the most loaded specimens, when the comparison is established between tests performed at the same room temperature. The specimens at 30 ºC had a higher strain rate absolute value after unloading mainly because the load was removed later (3000 hours) than the specimens at 20 ºC (2184 hours). In this matter, creep behaviour after unloading followed an inverse path compared

to loading, similar to a primary creep stage: the strain rate was high and decreased with time but had negative values. Then, the tests were ended (stopped) when the beginning of the secondary stage took place.

Some conclusions about the viscoelastic linearity of the PIR foam can be derived from **Figure 8**, where the creep compliance values calculated for the tests are displayed. As can be seen, creep compliance values follow the same path of the shear strain values (**Figure 7**), with the exception of one of the specimens subjected to 60% of the shear strength (at 20 ºC). Specimen C-L60-T20-2 showed creep compliance values close to the specimens subjected to 40% of the shear strength, a fact that is most likely attributed to the high variability occurring when load amplitudes are high, such is the case.

Figure 8 also reveals that creep compliance values increased with the shear stress applied, indicating nonlinear creep. In this context, a load amplitude corresponding to 30% of PIR shear strength was enough to induce a nonlinear creep response, a lower threshold value compared to the values obtained by Huang and Gibson [29] and Garrido *et al.* [16] in a high-density PUR foam. Huang and Gibson [29] concluded that the PUR foam tested had a linear viscoelastic behaviour below half the shear strength, while Garrido *et al.* [16] stated that a shear stress of 44% of the shear strength was high enough to cause nonlinear creep.

Finally, analysing the influence of temperature in the results, the values of the elastic shear strain γ_e were not significantly different between the tests at 20 ºC and at 30 ºC. Then, after loading, it can be noticed that the specimens tested at 20 ºC had a lower strain rate. However, that primary creep stage lasted longer, and with time the shear strain became slightly higher than the shear strain measured in specimens tested at 30 ºC. In the tests of Garrido *et al.* [16] on a PUR foam, the observed behaviour was contrary, with higher creep deformations achieved by the specimens when the temperature increased. However, as was mentioned before, PIR is an enhanced material in terms of thermal stability. The DMA test performed in the present work showed (see **Figure 2**) that the loss factor slightly decreases when the temperature increases, in the range of the common foam service temperatures. This fact is apparently the most plausible explanation for the better creep response detected in the specimens tested at 30 ºC.

4.3 Post-shear creep tests

Table 4 presents the results obtained in the 6 post-shear creep tests. The average values of G, τ_u and γ_u obtained in the monotonic-instantaneous shear tests (without creep effects) are taken as reference values, and therefore (see **Table 1**): G_{ref} = 2.77 MPa; $\tau_{u,ref}$ = 0.19 MPa; and $\gamma_{u,ref}$ = 0.193. Then, comparing the post-creep results

with the reference values, the applied creep load did not cause damage on the shear strength and stiffness of the PIR specimens. Material hardening can be detected in the post-creep mechanical properties, with higher values achieved for the shear modulus and ultimate shear strength. Material hardening also manifests itself in the less ductile and more brittle post-creep failure of the specimens, with lower values achieved for the ultimate shear strain.

5. ANALYTICAL MODELLING OF CREEP BEHAVIOUR

Accurate simulations of PUR subjected to shear creep loading by using the Findley's power law [30,31] was already demonstrated in literature [16,29], and therefore it is also considered in the present work for the analytical modelling of the PIR foam shear creep behaviour. In this section, the Findley's power law formulation is presented. Then, the parameters of the power law are determined based on the results obtained in the experimental campaign. The calibration of the parameters follows two approaches: i) shear strain of the PIR foam due to the creep effect is assumed to be independent of temperature; and ii) temperature influence is considered on the creep response.

5.1 Findley's power law

The Findley's power law is an empirical equation in which the shear strain due to the creep effect, γ_{cr}, varies as a power of the time (in hours) after loading is applied, *t*:

$$\gamma_{cr} = m \times \left(\frac{t}{t_0} \right)^n \tag{4}$$

In this formulation, the total shear strain is calculated from the following equation:

$$\gamma = \gamma_e + m \times \left(\frac{t}{t_0} \right)^n \tag{5}$$

where *m* is a creep amplitude coefficient depending on the applied stress and *n* is a time exponent coefficient, independent of stress and foam density. The coefficient *n* is assumed to be a material dependent for a given hygrothermal condition [29,48]. The values of both coefficients are calibrated from the experimental results obtained. t_0 is the time unit considered, so the time parameter can be normalized and the dimension consistency of Equation (5) assured. t_0 = 24 hours (1 day) is considered in the present work.

Calibration of the Findley's power law parameters from the experimental results was performed using the Nonlinear Generalized Reduced Gradient optimization algorithm of Lasdon *et al.* [49]. The automatic implementation of this algorithm is included in the Microsoft Excel Solver tool and its background theory can be consulted in detail in Reference [50]. The coefficients *m* and *n* are calculated aiming to minimize the sum *s*:

$$s = \sum_{i=1}^{t} \left| \gamma_{i,\text{exp}} - \gamma_{i,\text{num}} \right| \tag{6}$$

where γ_{exp} is the shear strain measured in the experimental tests, and γ_{num} is the shear strain given by the Findley's power law. The sum has the time step of 1 day.

For the unloading phase, the adopted analytical modelling of the foam relaxation can be useful for predicting, at a certain time, the residual deformation after the application of a creep load. To achieve that purpose, a primary analysis revealed that a satisfactory approximation between experimental and modelling values could be obtained considering the Findley's power law as well. The implemented analysis demonstrated that:

- After the unloading instant, the calculation of the creep deformation recovery from the Findley's power law should contemplate time after unloading, i.e. t is replaced by $t - t_{un}$, where t_{un} (in days) is the age at which unloading is done;
- The creep amplitude coefficient at the unloading phase, hereinafter designated as m_{un}, must assume a negative value, and a smaller absolute value compared to the loading phase;
- A modification in the time exponent coefficient n for the unloading phase is not necessary, and the value considered in the loading phase can be maintained. This fact sustains the notion, already mentioned, that n is a material constant for a given hygrothermal condition.

Thus, at the unloading stage, the calculation of the creep deformation recovery $\gamma_{cr,un}$ from the Findley's power law can be given by the following equation:

$$\gamma_{\text{cr,un}} = m_{\text{un}} \times \left(\frac{t - t_{\text{un}}}{t_0} \right)^n \tag{7}$$

Since the elastic deformation γ_e is completely recovered after unloading, Equation (5) is reduced to:

$$\gamma = \gamma_{\text{e}} + m \times \left(\frac{t_{\text{un}}}{t_0} \right)^n - \gamma_{\text{e}} + m_{\text{un}} \times \left(\frac{t - t_{\text{un}}}{t_0} \right)^n \tag{8}$$

or

$$\gamma = m \times \left(\frac{t_{un}}{t_0} \right)^n + m_{un} \times \left(\frac{t - t_{un}}{t_0} \right)^n \quad (9)$$

367

368 **5.2 Calibration assuming creep behaviour independent of temperature**

369 As could be observed in the shear strain results of **Figure 7** and in the DMA test of **Figure 2**, creep
370 deformations in PIR foam are slightly higher at 20 ºC compared to 30 ºC. The difference is not very significant,
371 and seems plausible to assume in modelling, at first hand, a simpler approach in which temperature does not
372 influence creep behaviour in the range of 20 ºC to 30 ºC.

373 **Figure 9** reveals the results achieved with this procedure, and a very satisfactory fitting can be identified
374 between experimental and modelling values. Especially for the tests at 30 ºC, which present less variability
375 compared to the ones at 20 ºC. **Table 5** shows the values calibrated for the coefficients *m* and *n*. The calibration
376 error is calculated through the following expression:

$$\text{error} = \frac{\sum_{i=1}^{t} \left| \gamma_{i,\text{exp}} - \gamma_{i,\text{num}} \right|}{\sum_{i=1}^{t} \gamma_{i,\text{exp}}} \quad (10)$$

377 **Figure 10** depicts the values calibrated for the coefficient *m* in function of the applied shear stress (τ / τ_{max}).
378 The trend curve that provided the best fit, among others that were tested, was the following empirical power law
379 with a regression factor $R^2 = 0.998$:

$$m = a \times \left(\frac{\tau}{\tau_{max}} \right)^b \quad (11)$$

380 with $a = 0.0452$ and $b = 1.684$.

381 As was proved in the tests of Huang and Gibson [29], the coefficient *m* is directly proportional to the applied
382 stress when creep is linear. However, linear creep could not be detected in the experimental campaign carried out
383 in the present work, and this fact seems to explain the power law variation of *m* in **Figure 10** with the applied
384 stress.

385 Then, it was later concluded in the calibration procedure of m_{un} that: i) m_{un} is directly proportional to *m*;
386 and ii) determination of m_{un} must include the age t_{un} (in days) at which unloading is done. At the end, the following
387 empirical expression was derived for m_{un}:

$$m_{un} = -0.004 \times m \times \left(\frac{t_{un}}{t_0} \right) \tag{12}$$

388 or

$$m_{un} = -1.808 \times 10^{-4} \times \left(\frac{\tau}{\tau_{max}} \right)^{1.684} \times \left(\frac{t_{un}}{t_0} \right) \tag{13}$$

389 when Equation (11) is incorporated.

390 The results of this modelling approach for the unloading stage are depicted on **Figure 9**. As can be seen,
391 the power law curves reflect the strain rate tendency for all the stress levels and for both tests at 20 ºC and 30 ºC.
392 For the elastic strain γ_e, it was considered $\gamma_e = \tau / G$, with G = 2.77 MPa. The value adopted for the shear modulus
393 G is the average value obtained in the shear failure experimental tests which depicted a transverse shear failure
394 mode (see **Table 1**).

395 ### 5.3 Calibration assuming creep behaviour dependent on temperature

396 An analytical modelling approach is presented in this section in which the calculation of creep shear strain
397 from the Findley's power law depends on temperature. For that purpose, and since the tests were developed at two
398 temperatures (20 ºC and 30 ºC), some parameters of the Findley's power law in this approach become now linearly
399 dependent on temperature. A linear dependency between temperature and the viscoelastic behaviour of the PIR
400 foam was depicted in the DMA test of **Figure 2**, for a temperature range between 0 ºC and 40 ºC.

401 In this analysis, it was assumed that creep behaviour is dependent on temperature, and therefore a
402 calibration procedure was implemented, as in Section 5.2, to obtain values for the coefficients m and n for each
403 test series (see **Table 6**). In the following, Equation (14) could be derived for coefficient n, depending on
404 temperature T (in Kelvin):

$$n = -0.001248 \times T + 0.6855 \tag{14}$$

405 The best fit for the coefficient m variation with the stress level is a power law similar to the one presented
406 in Equation (11), whose representation for the tests at 20 ºC and at 30 ºC are depicted in **Figure 11**. In that
407 procedure, it was noticed that coefficient b of the power law (see Equation (11)) did not vary significantly with
408 temperature, and good results could be achieved through the consideration of a constant value (b = 1.6245).

409 For coefficient a, a linear expression was adopted in function of temperature T (in Kelvin), according to
410 Equation (15):

$$a = -0.00025 \times T + 0.117 \quad (15)$$

Finally, **Figure 9** illustrates the new Findley's power law curves corresponding to this approach, where the influence of temperature is considered in the creep shear strain analytical calculation. A slight improvement occurs, with the model curves closer to the experimental values. This enhancement is more perceptible in the tests at 20 ºC, particularly the ones carried out with $\tau / \tau_{max} = 0.4$. For other temperature ranges, if they are within 0 ºC to 40 ºC, the advantages regarding the use of this temperature dependant approach are expected to be more evident.

6. CONCLUSIONS

An experimental campaign was developed to assess shear strength and the shear creep behaviour of a rigid low-density closed-cell PIR foam, commonly used in the insulation of structural sandwich panels. Temperature influence on the creep deformations was also evaluated through standardized pure shear tests performed at 20 ºC and at 30 ºC, for different stress levels (20% to 60% of the average shear strength). Then, an analytical model based on the Findley's power law was calibrated to the experimental results, for both loading and unloading stages. In this context, two modelling approaches were considered: i) a temperature independent approach, suitable to use in the 20 ºC to 30 ºC service temperature range; and ii) a temperature dependent approach, which is expected to give more accurate results for wider service temperature ranges (within 0º C to 40 ºC). The main conclusions that can be derived from the work in this paper are the following:

- PIR is a thermosetting polymer with a very high thermal stability, particularly in the common service temperature ranges. The DMA test carried out in the present study showed results similar to those typically seen in thermosetting polymers with crystalline structure, known for their almost perfectly regular and periodic molecular arrangement. The DMA revealed that from 0 ºC to 40 ºC the loss factor of PIR decreases slightly with the temperature increase, indicating an improvement in the viscoelastic behaviour of PIR in that temperature range;
- Even for creep loading corresponding to 60% of the average shear strength, no PIR foam specimen failed during the creep tests, which were maintained until at least 90 days after loading was applied;
- A stress level corresponding to 30% of the PIR average shear strength was enough to induce a nonlinear creep response;
- Creep deformations were slightly higher in the tests performed at 20 ºC compared to the ones performed at 30 ºC, matching the viscoelastic observed in the DMA test of the PIR foam;

- Material hardening can be detected in the post-creep mechanical properties, with higher values achieved for the shear modulus and ultimate shear strength, and lower values achieved for the ultimate shear strain;
- Analytical modelling of the PIR foam creep behaviour through the Findley's power law provided good results and a very satisfactory fitting to the experimental values was noticed;
- In the temperature range between 20 ºC and 30 ºC, Findley's power law parameter calculation could be extended in order to account temperature's influence in the PIR foam creep deformations.

ACKNOWLEDGEMENTS

This work is part of the research project "EasyFloor – Development of composite sandwich panels for rehabilitation of floor buildings", involving the company ALTO – Perfis Pultrudidos, Lda., CERis/Instituto Superior Técnico and ISISE/University of Minho, supported by FEDER funds through the Operational Program for Operational Program for Competitiveness and Internationalization (POCI) and the Portuguese National Innovation Agency (ANI) - project no. 3480 (POCI-01-0247-FEDER-003480). The second author acknowledge the grant SFRH/BSAB/150266/2019 provided by FCT, financed by European Social Fund and by national funds through the FCT/MCTES. Acknowledgments are extended to LEST – Laboratório de Estruturas for their material support. The contribution of the Department of Mechanical Engineering of the University of Minho is also gratefully acknowledged in the person of Engineer Pedro Ribeiro. Lastly, the authors would like to thank SIKA Company for suppling the adhesive.

REFERENCES

1. Vitkauskiene, I., et al., *Synthesis and physical-mechanical properties of polyurethane-polyisocyanurate foams based on PET-waste-derived modified polyols*. Journal of Cellular Plastics, 2011. **47**(5): p. 467-482.
2. Zatorski, W., Z.K. Brzozowski, and A. Kolbrecki, *New developments in chemical modification of fire-safe rigid polyurethane foams*. Polymer Degradation and Stability, 2008. **93**(11): p. 2071-2076.
3. Czupryński, B., J. Paciorek-Sadowska, and J. Liszkowska, *Properties of rigid polyurethane-polyisocyanurate foams modified with the selected fillers*. Journal of Applied Polymer Science, 2010. **115**(4): p. 2460-2469.
4. Du, M., C. He, and C. Zhou, *Flame retardant effect of isocyanate trimer on polyisocyanurate foam*. Journal of Polymer Science and Engineering, 2018. **1**(1).
5. Cabulis, U., et al., *Rapeseed oil-based rigid polyisocyanurate foams modified with nanoparticles of various type*. Polimery, 2014. **59**(3): p. 207-212.
6. Chen, K., et al., *Preparation and characterization of highly thermostable polyisocyanurate foams modified with epoxy resin*. Journal of Applied Polymer Science, 2016. **133**(13).
7. Tuwair, H., et al., *Evaluation of sandwich panels with various polyurethane foam-cores and ribs*. Composites Part B: Engineering, 2015. **79**: p. 262-276.
8. Wang, J., et al., *A failure mechanism based model for numerical modeling the compression-after-impact of foam-core sandwich panels*. Composites Science and Technology, 2017. **151**: p. 258-267.
9. Fam, A. and T. Sharaf, *Flexural performance of sandwich panels comprising polyurethane core and GFRP skins and ribs of various configurations*. Composite Structures, 2010. **92**(12): p. 2927-2935.
10. Paciorek-Sadowska, J., B. Czupryński, and J. Liszkowska, *Boron-containing fire retardant rigid polyurethane–polyisocyanurate foams: Part II–preparation and evaluation*. Journal of Fire Sciences, 2015. **33**(1): p. 48-68.
11. Kang, M.J., et al., *Liquid nucleating additives for improving thermal insulating properties and mechanical strength of polyisocyanurate foams*. Journal of Materials Science, 2010. **45**(19): p. 5412-5419.
12. Wang, Y.C. and A. Foster, *Experimental and numerical study of temperature developments in PIR core sandwich panels with joint*. Fire Safety Journal, 2017. **90**: p. 1-14.
13. Mohamed, M., et al., *Manufacturing and characterization of polyurethane based sandwich composite structures*. Composite Structures, 2015. **123**: p. 169-179.
14. De Matteis, G. and R. Landolfo, *Structural behaviour of sandwich panel shear walls: An experimental analysis*. Materials and Structures, 1999. **32**(5): p. 331-341.
15. Arruda, M.R.T., et al., *Numerical modelling of the creep behaviour of GFRP sandwich panels using the Carrera Unified Formulation and Composite Creep Modelling*. Composite Structures, 2018. **183**: p. 103-113.
16. Garrido, M., J.R. Correia, and T. Keller, *Effect of service temperature on the shear creep response of rigid polyurethane foam used in composite sandwich floor panels*. Construction and Building Materials, 2016. **118**: p. 235-244.
17. Chen, K., et al., *Effect of stoichiometry on the thermal stability and flame retardation of polyisocyanurate foams modified with epoxy resin*. Polymer Degradation and Stability, 2018. **150**: p. 105-113.
18. Gao, L., et al., *Synergistic effect of expandable graphite, diethyl ethylphosphonate and organically-modified layered double hydroxide on flame retardancy and fire behavior of polyisocyanurate-polyurethane foam nanocomposite*. Polymer Degradation and Stability, 2014. **101**: p. 92-101.
19. Hejna, A., et al., *Structure, mechanical, thermal and fire behavior assessments of environmentally friendly crude glycerol-based rigid polyisocyanurate foams*. Journal of Polymers and the Environment, 2018. **26**(5): p. 1854-1868.

20. Kim, Y.H., et al., *Effects of liquid-type silane additives and organoclay on the morphology and thermal conductivity of rigid polyisocyanurate-polyurethane foams*. Journal of Applied Polymer Science, 2012. **124**(4): p. 3117-3123.

21. Kurańska, M., et al., *Bio-based polyurethane-polyisocyanurate composites with an intumescent flame retardant*. Polymer Degradation and Stability, 2016. **127**: p. 11-19.

22. Liu, Y., J. He, and R. Yang, *The effects of aluminum hydroxide and ammonium polyphosphate on the flame retardancy and mechanical property of polyisocyanurate–polyurethane foams*. Journal of Fire Sciences, 2015. **33**(6): p. 459-472.

23. Park, D.H., et al., *Effects of isocyanate index and environmentally-friendly blowing agents on the morphological, mechanical, and thermal insulating properties of polyisocyanurate-polyurethane foams*. Macromolecular Research, 2013. **21**(8): p. 852-859.

24. Xu, Q., et al., *The effect of the trimerization catalyst on the thermal stability and the fire performance of the polyisocyanurate-polyurethane foam*. Fire and Materials, 2018. **42**(1): p. 119-127.

25. Ashby, M.F. and R.M. Medalist, *The mechanical properties of cellular solids*. Metallurgical Transactions A, 1983. **14**(9): p. 1755-1769.

26. Hawkins, M.C., B. O'Toole, and D. Jackovich, *Cell morphology and mechanical properties of rigid polyurethane foam*. Journal of Cellular Plastics, 2005. **41**(3): p. 267-285.

27. Goods, S.H., et al., *Mechanical properties and energy absorption characteristics of a polyurethane foam*. SAND97-8490, Sandia National Laboratories, 43 pp., 1997.

28. Witkiewicz, W. and A. Zieliński, *Properties of the polyurethane (PU) light foams*. Advances in Materials Science, 2006. **6**(2): p. 35-51.

29. Huang, J.S. and L.J. Gibson, *Creep of polymer foams*. Journal of Materials Science, 1991. **26**(3): p. 637-647.

30. Findley, W.N., *Mechanism and mechanics of creep of plastics and stress relaxation and combined stress creep of plastics*. Division of Engineering, Brown University, 16 pp., 1960.

31. Lai, J.S.Y. and W.N. Findley, *Elevated temperature creep of polyurethane under nonlinear torsional stress with step changes in torque*. Transactions of the Society of Rheology, 1973. **17**(1): p. 129-150.

32. El Ghezal, M.I., Y. Maalej, and I. Doghri, *Micromechanical models for porous and cellular materials in linear elasticity and viscoelasticity*. Computational Materials Science, 2013. **70**: p. 51-70.

33. Crawford, D.M., R.G. Bass, and T.W. Haas, *Strain effects on thermal transitions and mechanical properties of thermoplastic polyurethane elastomers*. Thermochimica Acta, 1998. **323**(1-2): p. 53-63.

34. Garrido, M., J.R. Correia, and T. Keller, *Effects of elevated temperature on the shear response of PET and PUR foams used in composite sandwich panels*. Construction and Building Materials, 2015. **76**: p. 150-157.

35. Briody, C., et al., *Prediction of compressive creep behaviour in flexible polyurethane foam over long time scales and at elevated temperatures*. Polymer Testing, 2012. **31**(8): p. 1019-1025.

36. Javni, I., W. Zhang, and Z.S. Petrović, *Soybean-oil-based polyisocyanurate rigid foams*. Journal of Polymers and the Environment, 2004. **12**(3): p. 123-129.

37. Stirna, U., U. Cabulis, and I. Beverte, *Water-blown polyisocyanurate foams from vegetable oil polyols*. Journal of Cellular Plastics, 2008. **44**(2): p. 139-160.

38. Andersons, J., et al., *Anisotropy of the stiffness and strength of rigid low-density closed-cell polyisocyanurate foams*. Materials & Design, 2016. **92**: p. 836-845.

39. Andersons, J., et al., *Modeling the mode I fracture toughness of anisotropic low-density rigid PUR and PIR foams*. International Journal of Fracture, 2017. **205**(1): p. 111-118.

40. Sena-Cruz, J.M., et al., *A hybrid cementitious based-G/CFRP sandwich panel: concept, design and initial outcomes*. in *12th International Conference on Sandwich Structures*. 2018. Lausanne, Switzerland: ICSS.

41. *ASTM C365/C365M:2016*, in *Standard test method for flatwise compressive properties of sandwich cores*. West Conshohocken (United States): ASTM International.

554 42. *ASTM C297/C297M:2016*, in *Standard test method for flatwise tensile strength of sandwich*
555 *constructions*. West Conshohocken (United States): ASTM International.

556 43. Sun, T., et al., *Phase transitions of poly (ethylene terephthalate-co-p-hydroxybenzoic acid) liquid crystal*
557 *by dynamic mechanical analysis*. Polymer, 1989. **30**(7): p. 1257-1261.

558 44. *ASTM C273/C273M:2016*, in *Standard test method for shear properties of sandwich core materials*. West
559 Conshohocken (United States): ASTM International.

560 45. *ISO 1922:2012*, in *Rigid cellular plastics – Determination of shear strength*. Geneva (Switzerland):
561 Technical Committee ISO/TC 61/SC 10.

562 46. Escusa, G.G., et al., *Shear behaviour of polyurethane foam*. in *6th Asia-Pacific Conference on FRP in*
563 *Structures*. 2017. Singapore: APFIS.

564 47. Courtney, T.H., *Mechanical behavior of materials*. 2005. Illinois (United States): Waveland Press.

565 48. Costa, I.G. and J.A.O. Barros, *Tensile creep of a structural epoxy adhesive: experimental and analytical*
566 *characterization*. International Journal of Adhesion & Adhesives, 2015. **59**: p. 115-124.

567 49. Lasdon, L.S., et al., *Design and testing of a generalized reduced gradient code for nonlinear*
568 *programming*. ACM Transactions on Mathematical Software, 1978. **4**(1): p. 34-50.

569 50. Coello Coello, C.A., G.B. Lamont, and D.A. Van Veldhuizen, *Evolutionary algorithms for solving multi-*
570 *objective problems*. 2007. New York (United States): Springer.

571

Figueira, D.; Sena-Cruz, J.; Pereira, E.; Valente, I.; Barros, J.; Castro, F.; Soares, D. (2019) "Influence of service temperature on shear creep behaviour of a rigid low-density closed-cell PIR foam" Construction & Building Materials, 225: 1052–1063.
DOI: 10.1016/j.conbuildmat.2019.07.337

572 **LIST OF TABLES**

582

583 **Table 1 -** Results of the shear failure tests on PIR foam specimens.

Specimen	ρ [kg/m^3]	G [MPa]	τ_u [MPa]	γ_u [-]	**Failure mode** ([1])
F1	38.81	2.68	0.13	0.075	FM1
F2	37.67	2.75	0.16	0.139	FM1
F3	38.43	2.77	0.19	0.190	FM2
F4	35.58	2.81	0.18	0.178	FM2
F5	38.19	2.64	0.19	0.173	FM1
F6	36.62	2.74	0.19	0.211	FM2
Average	37.55	2.73	0.17	0.161	All
CoV (%)	2.98	2.06	13.6	27.4	
Average	36.88	2.77	0.19	0.193	FM2
CoV (%)	3.19	1.03	3.1	7.1	
Average	38.22	2.69	0.16	0.129	FM1
CoV (%)	1.22	1.69	16.3	31.5	

([1]) FM1 – Failure mode governed by a shear crack parallel to the steel plates; FM2 – Failure mode governed by a shear crack transverse to the steel plates.

584

585

586 **Table 2 -** Values of shear strain γ over time t (in hours) in the shear creep tests on the PIR foam at 20 ºC.

Specimen	**Creep load (% of shear strength)**	γ_e (t = 0)	$\gamma_{e,expected}$ (t = 0)	γ_c (t = 2184)	γ_{un} (t = 2184)	γ_{end} (t = 3168)
C-L20-T20-1	20	0.012	0.013	0.027	0.015	0.012
C-L20-T20-2		0.013		0.026	0.015	0.011
C-L40-T20-1	40	0.028	0.027	0.065	0.042	0.033
C-L40-T20-2		0.028		0.070	0.044	0.035
C-L60-T20-1	60	0.042	0.040	0.134	0.093	0.077
C-L60-T20-2		0.036		0.099	0.068	0.055

587

588

589 **Table 3 -** Values of shear strain γ over time t (in hours) in the shear creep tests on the PIR foam at 30 ºC.

Specimen	Creep load (% of shear strength)	γ_e (t = 0)	$\gamma_{e,expected}$ (t = 0)	γ (t = 2184)	γ_c (t = 3000)	γ_{un} (t = 3000)	γ_{end} (t = 4080)
C-L20-T30-1	20	0.012	0.013	0.025	0.026	0.013	0.008
C-L20-T30-2		0.012		0.026	0.028	0.015	0.011
C-L30-T30-1	30	0.021	0.020	0.042	0.044	0.025	0.015
C-L30-T30-2		0.021		0.044	0.047	0.026	0.016
C-L40-T30-1	40	0.029	0.027	0.061	0.065	0.034	0.020
C-L40-T30-2		0.026		0.065	0.070	0.041	0.029

590

591

592 **Table 4 -** Comparison of results obtained in the post-shear creep tests with the (before creep) shear tests, up to
593 failure (reference values).

Specimen	G [MPa]	τ_u [MPa]	γ_u [-]	**Failure mode** ([1])	G / G_{ref}	$\tau_u / \tau_{u,ref}$	$\gamma_u / \gamma_{u,ref}$
C-L20-T30-1	2.89	0.20	0.169	FM2	1.04	1.05	0.88
C-L20-T30-2	3.24	0.22	0.190	FM2	1.17	1.16	0.98
C-L30-T30-1	3.05	0.20	0.175	FM2	1.10	1.05	0.91
C-L30-T30-2	3.08	0.20	0.174	FM2	1.11	1.05	0.90
C-L40-T30-1	2.89	0.19	0.184	FM1	1.04	1.00	0.95
C-L40-T30-2	3.33	0.21	0.140	FM2	1.20	1.11	0.73
Average	3.08	0.20	0.172	all	1.11	1.07	0.89
CoV (%)	5.32	4.64	9.23		5.41	4.80	8.91
Average	3.12	0.21	0.170	FM2	1.12	1.08	0.88
CoV (%)	4.92	3.88	9.66		4.99	4.11	9.34

([1]) FM1 – Failure mode governed by a shear crack parallel to the steel plates; FM2 – Failure mode governed by a shear crack transverse to the steel plates.

594

595

596 **Table 5 -** Coefficients *m* and *n* calibrated from the experimental tests, assuming creep behaviour independent of
597 temperature.

m	*n*	**Creep load (% of shear strength)**	**Temperature** [ºC]	**Error** [%]
0.0031		20		5.50
0.0094	0.3076	40	20	5.66
0.0199		60		4.21
0.0031		20		1.95
0.0058	0.3076	30	30	1.83
0.0094		40		2.26

598

599

600 **Table 6 -** Coefficients *m* and *n* calibrated from the experimental tests, assuming creep behaviour dependent on
601 temperature.

m	*n*	**Creep load (% of shear strength)**	**Temperature** [ºC]	**Error** [%]
0.0032		20		2.75
0.0099	0.3197	40	20	2.85
0.0191		60		3.37
0.0030		20		1.96
0.0058	0.3072	30	30	0.86
0.0093		40		0.88

602

603

Figueira, D.; Sena-Cruz, J.; Pereira, E.; Valente, I.; Barros, J.; Castro, F.; Soares, D. (2019) "Influence of service temperature on shear creep behaviour of a rigid low-density closed-cell PIR foam" Construction & Building Materials, 225: 1052–1063.
DOI: 10.1016/j.conbuildmat.2019.07.337

LIST OF FIGURES

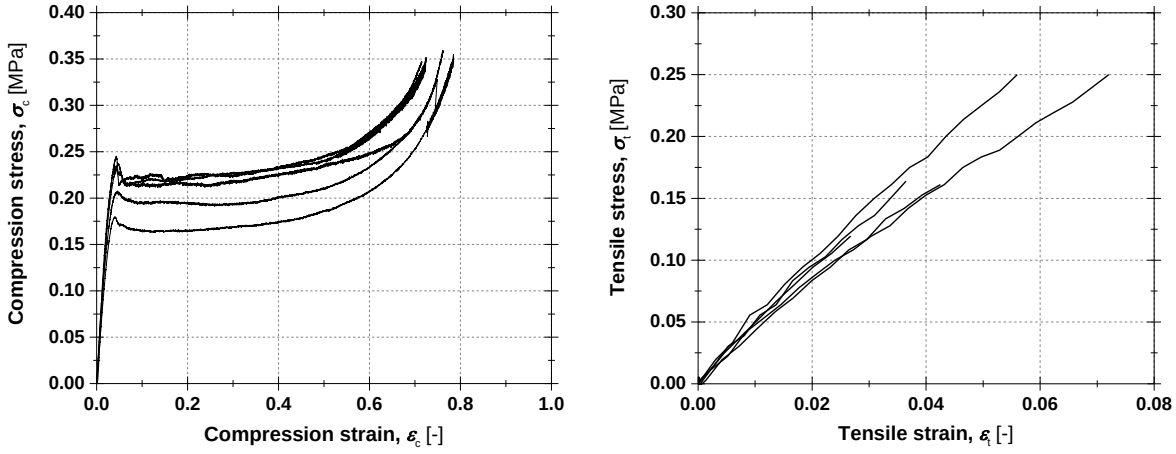

(a) (b)

626 **Figure 1 -** Stress – strain curves acquired in the PIR foam failure tests: (a) compression; (b) tensile.

627

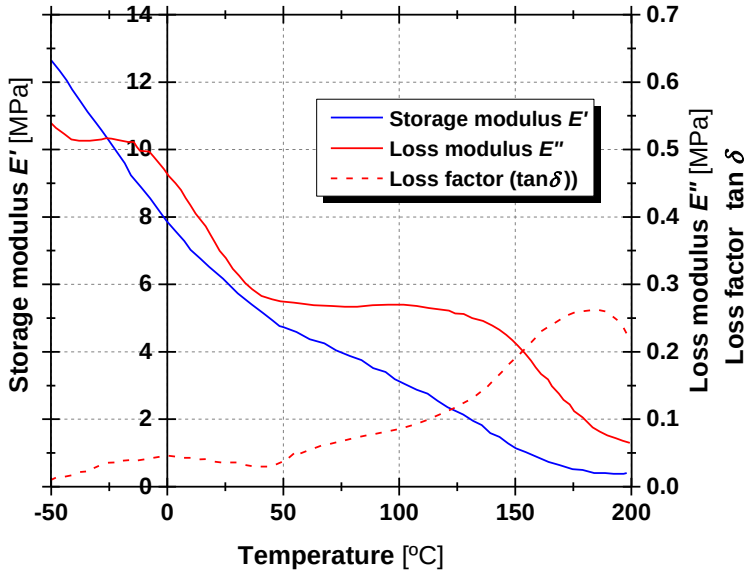

628

629 **Figure 2 -** Typical results of the DMA test carried out in the PIR foam (storage modulus, loss modulus and loss

630 factor from -50 ºC to 200 ºC).

631

Figueira, D.; Sena-Cruz, J.; Pereira, E.; Valente, I.; Barros, J.; Castro, F.; Soares, D. (2019) "Influence of service temperature on shear creep behaviour of a rigid low-density closed-cell PIR foam" Construction & Building Materials, 225: 1052–1063.
DOI: 10.1016/j.conbuildmat.2019.07.337

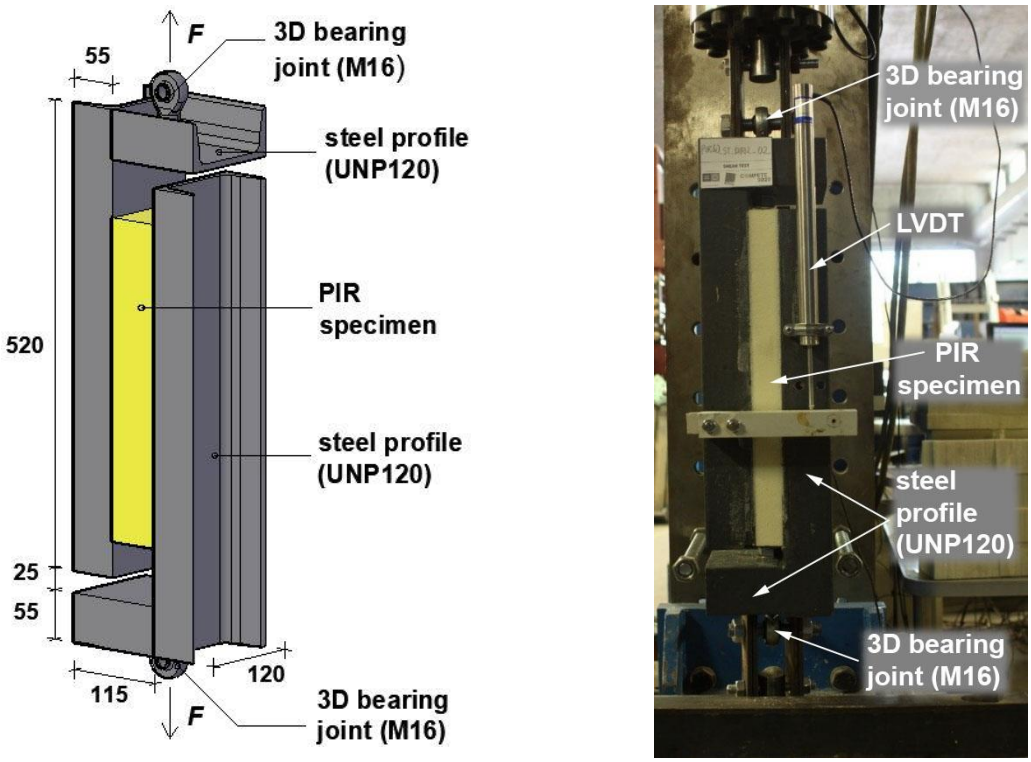

(a) (b)

Figure 3 - Test setup for the assessment of the PIR foam shear strength: (a) test fixture (dimensions in [mm]); (b) test configuration with the LVDT.

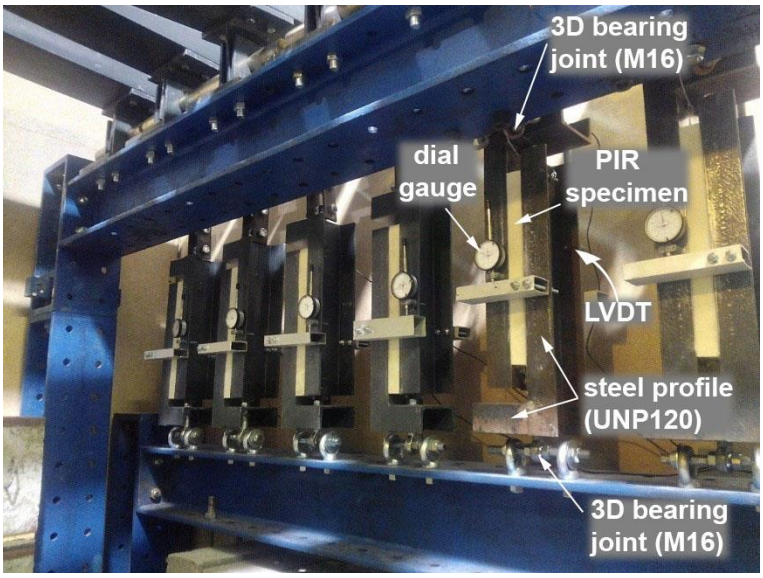

(a)

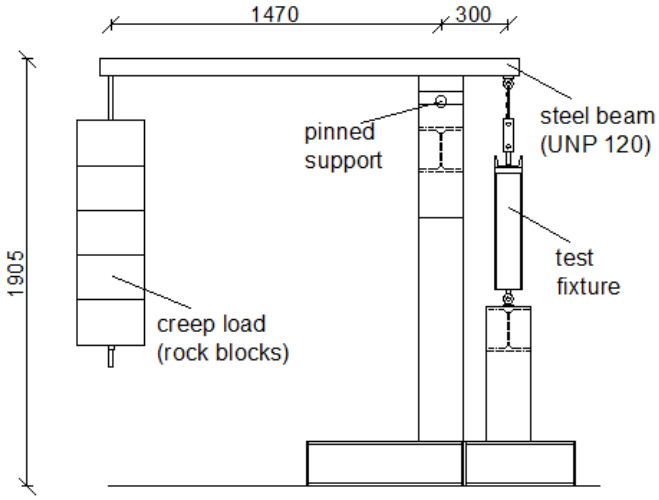

(b)

Figure 4 - Setup of the shear creep tests on the PIR foam: (a) front view; (b) schematic representation (dimensions in [mm]).

(a) (b)

642 **Figure 5 -** Failure modes identified in the tests performed to assess shear strength of the PIR foam: (a) FM1 -

643 shear crack parallel to the steel plates; (b) FM2 - transverse shear crack.

644

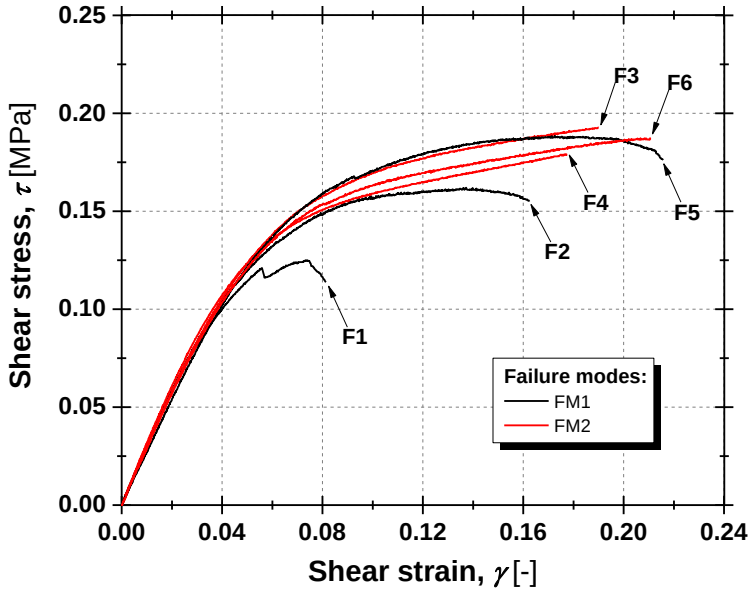

Figure 6 - Shear stress – strain curves acquired in the PIR foam failure tests.

Figueira, D.; Sena-Cruz, J.; Pereira, E.; Valente, I.; Barros, J.; Castro, F.; Soares, D. (2019) "Influence of service temperature on shear creep behaviour of a rigid low-density closed-cell PIR foam" Construction & Building Materials, 225: 1052–1063.
DOI: 10.1016/j.conbuildmat.2019.07.337

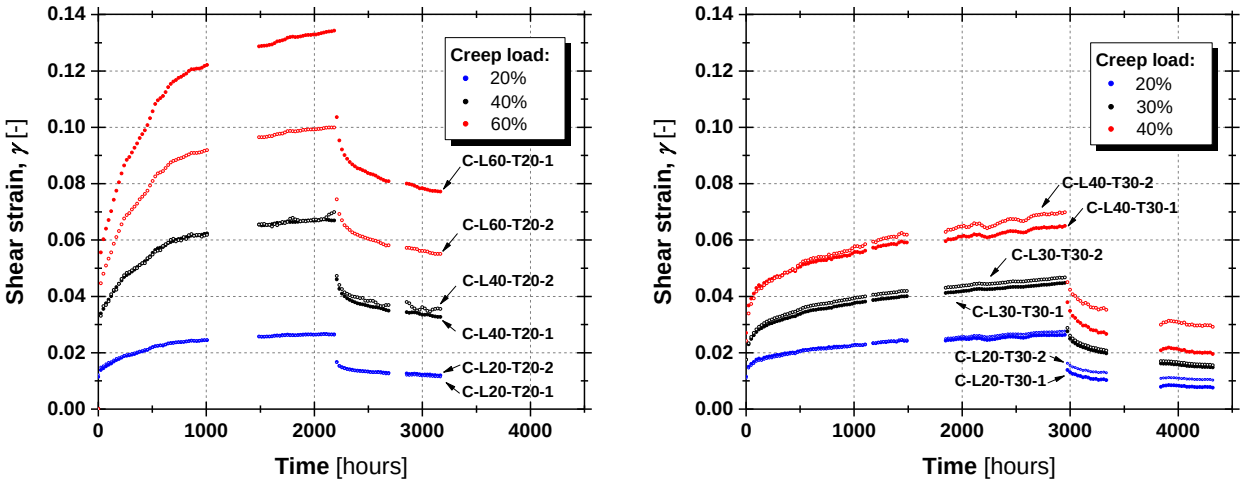

Figure 7 - Results of shear strain over time obtained in the shear creep tests on the PIR foam for different load amplitudes: (a) at 20 ºC; (b) at 30 ºC.

Figueira, D.; Sena-Cruz, J.; Pereira, E.; Valente, I.; Barros, J.; Castro, F.; Soares, D. (2019) "Influence of service temperature on shear creep behaviour of a rigid low-density closed-cell PIR foam" Construction & Building Materials, 225: 1052–1063.
DOI: 10.1016/j.conbuildmat.2019.07.337

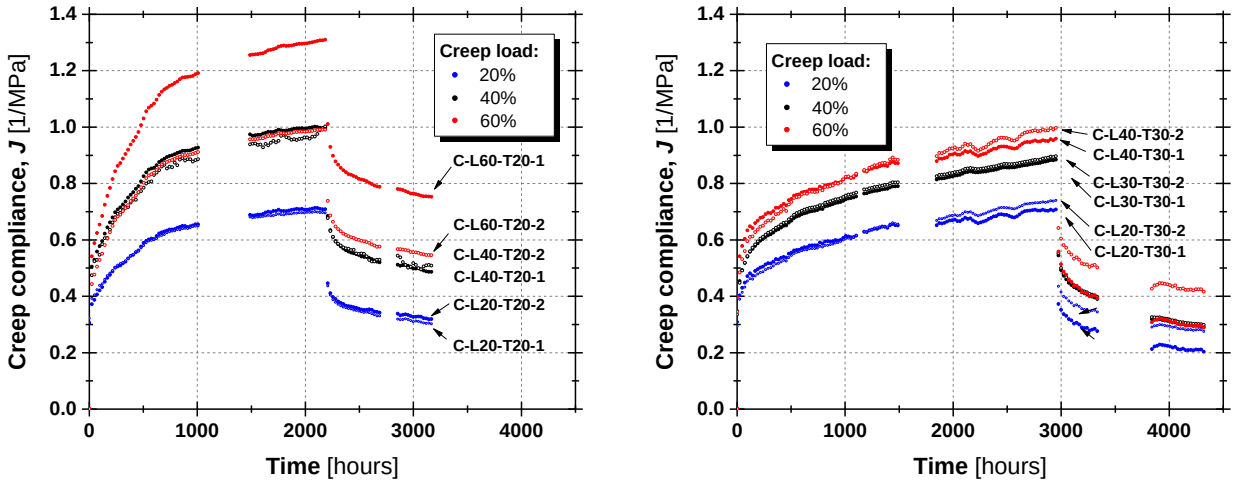

(a) (b)

Figure 8 - Results of creep compliance over time obtained in the shear creep tests on the PIR foam for different load amplitudes: (a) at 20 ºC; (b) at 30 ºC.

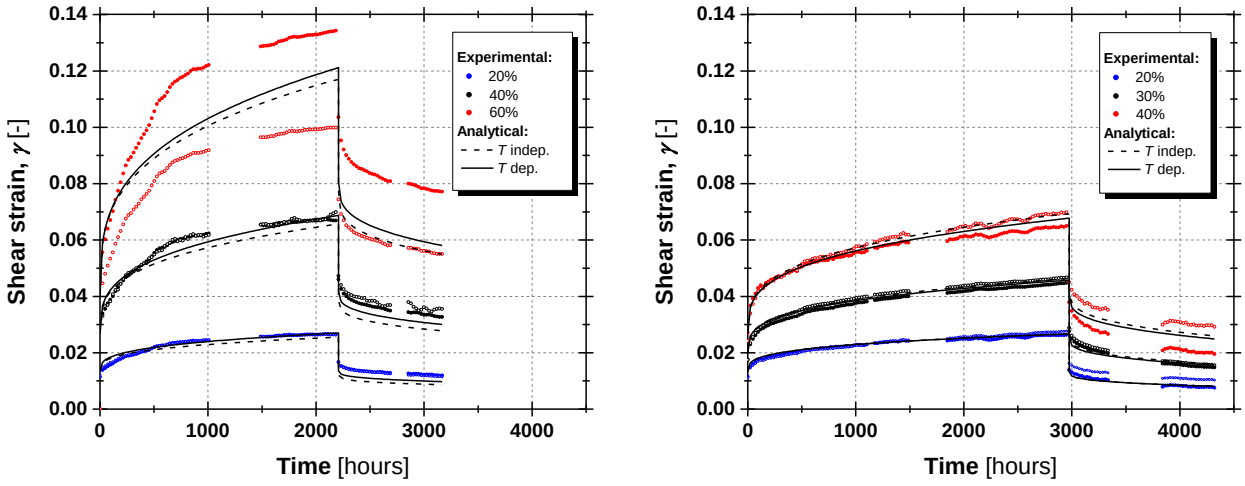

658 **Figure 9 -** Findley's power law numerical values adjusted to the experimental creep shear strain values: (a) at
659 20 ºC; (b) at 30 ºC.

660

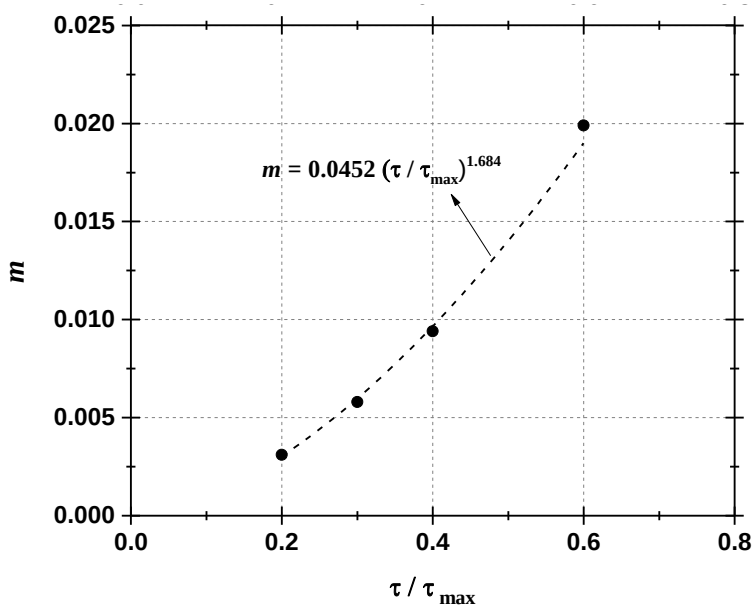

661

662 **Figure 10 -** Variation of the Findley's power law coefficient *m* as a function of the applied creep load (τ / τ_{max}),
663 assuming temperature does not affect creep behaviour.

664

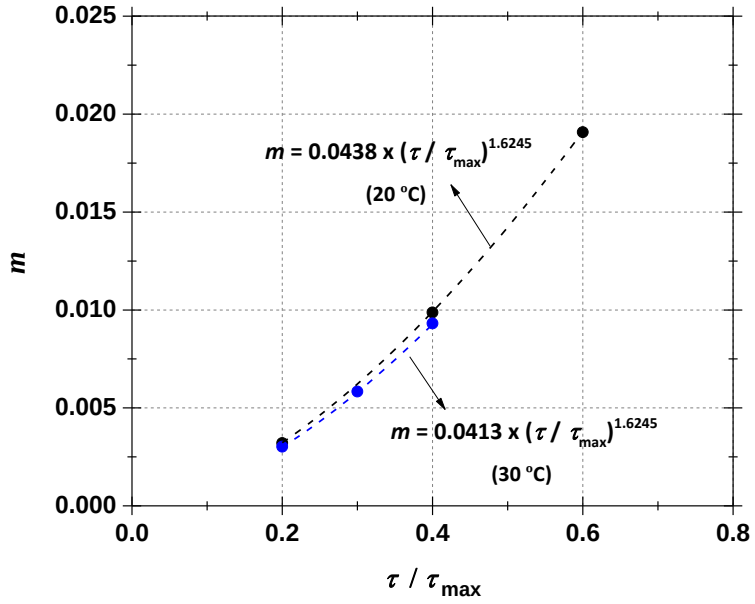

Figure 11 - Variation of the Findley's power law coefficient m as a function of the applied creep load (τ / τ_{max}), assuming temperature affects creep behaviour.